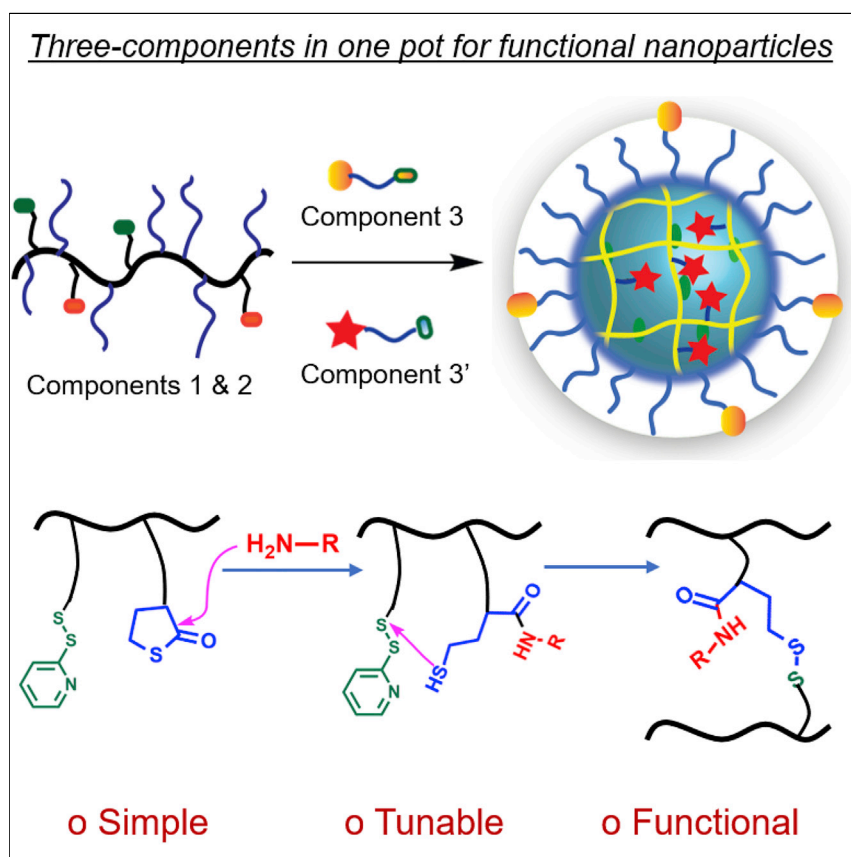


## Article

# Three-Component Sequential Reactions for Polymeric Nanoparticles with Tailorable Core and Surface Functionalities



Functional organic nanoparticles were prepared through a one-pot, three-component sequential reaction between small molecules and polymers with concurrent functionalization and crosslinking. This simple, scalable, and green process affords nanoparticles with size control, tunable surface and core functionalities, and high encapsulation stability with triggerable molecular release features.

Bin Liu, S. Thayumanavan

thai@chem.umass.edu

## HIGHLIGHTS

A simple one-pot multi-component reaction was developed for nanoparticle synthesis

Methodology offers concurrent surface and core functionalization capabilities

Nanoparticles exhibit tunability in size and encapsulation stability

Encapsulation is specifically compromised due to the triggerable release features

Article

# Three-Component Sequential Reactions for Polymeric Nanoparticles with Tailorable Core and Surface Functionalities

Bin Liu<sup>1</sup> and S. Thayumanavan<sup>1,2,3,4,\*</sup>

## SUMMARY

Efficient strategies for the preparation of nanostructures with tailorable functionalities have implications in enhancing the repertoire of nanomaterials in many applications. Multi-component reactions (MCRs) are very attractive because they are synthetically simple while providing unique access to incorporation of functional groups onto a system. This highly efficient process has not been brought to bear in the preparation of functional polymeric nanostructures. In this paper, we report a three-component sequential reaction that is capable of concurrently functionalizing the core and the surface of the nanoparticles and crosslinking the polymeric assemblies, along with excellent control over size (~10 nm to ~1 μm). Variations in core offer the opportunity to optimize the host-guest properties for non-covalent drug encapsulation, while the surface features provide the ability to tune interfacial interactions and achieve organelle targeting in cells. Encapsulation of drug molecules and their triggered release features have been utilized for intracellular drug delivery.

## INTRODUCTION

Nanoscale assemblies with sophisticated properties have attracted tremendous interest because of the potential applications in different fields such as drug delivery, biomedical diagnostics, and theranostics.<sup>1–5</sup> Scaffolds such as inorganic nanoparticles (NPs),<sup>6,7</sup> liposomes,<sup>8</sup> dendrimers,<sup>9</sup> polymeric assemblies,<sup>10–15</sup> and polymer-based NPs<sup>10–16</sup> have been explored for this purpose. Among these, amphiphilic block copolymer-based assemblies have been extensively studied because of their water solubility and non-covalent encapsulation capabilities of hydrophobic guest molecules in aqueous phase.<sup>10–16</sup> These features are particularly important for therapeutic applications, where the ability to load hydrophobic drug molecules into a water-dispersible nanoassembly is critical for overcoming some of the pharmacokinetic limitations of conventional drug formulations.<sup>17–20</sup> Block polymeric micelles contain well-defined core-shell structure with hydrophobic polymer cores and water-soluble polymer shells. In order to achieve efficient drug encapsulation inside the core of the block polymer micelles, it requires the guest molecules to overcome the barrier formed by the shell layer and the soft-glassy core polymer block. There are usually two methods for drug encapsulation, which is based on the dissolution of the drug molecules and the block copolymers in a water-miscible organic solvent together with subsequent addition of water and further removal of the organic solvent by evaporation or dialysis to efficiently decrease the energy barrier for the drug molecules to penetrate from the micelle shell to the glassy hydrophobic core.<sup>21–24</sup> However, these methods are not suitable for scalable production as physical factors (e.g., diffusion and solvent exchange rate) are influenced heavily by the scales during

## The Bigger Picture

Nanomedicine offers a promising approach for targeted therapeutics, such as in cancer. The complexity of biological barriers, however, presents a significant challenge in designing efficacious drug carriers. The key criteria that define highly efficient nanoparticles include (1) simple preparative chemistry that ultimately offers scalability, size control, and surface functionalization to optimally interface with biological systems to achieve the desired cellular targeting and (2) host-guest characteristics with good encapsulation stability that obviates premature drug release. In this work, we present a simple method for preparing functional nanoparticles through a one-pot, sequential multi-component reaction that exhibits convenient tunability in size, surface functionalities, and high encapsulation stability with triggerable release characteristics. The combination of these features highlights the potential of these nanoparticles in biomedicine.

the drug incorporation processes. Furthermore, there is also an environmental cost associated with using organic co-solvents in a process that is primarily driven by the propensity of the host assembly to self-assemble in water.<sup>21–24</sup>

Also, most disease models have disparate requirements in features such as size and surface functionalities to optimize their circulation time as well as tissue, cellular, and sub-cellular targeting.<sup>25–27</sup> Note, however, that it is difficult to tune the size of micelles from one polymeric precursor in the case of block copolymers, as the assembly size here is controlled by the relative block composition and the block length under equilibrium conditions<sup>23,24,28,29</sup>; i.e., a polymer with the specific structure usually affords a micelle with a well-defined size.<sup>23,24,28,29</sup> Therefore, when block copolymer micellar assemblies with different sizes are desired, a series of different polymers need to be designed and synthesized, which is time consuming and laborious.<sup>30</sup> In fact, it is difficult to prepare block-copolymer-based micelles with small ( $d < 20$  nm) and big ( $d > 100$  nm) sizes.<sup>28–32</sup> Moreover, the surface functional groups, which are often used for targeting purposes, must be specifically installed at the end of the hydrophilic terminus.<sup>31,32</sup> By the extension of this feature, for installing few different surface functionalities, polymers with these different terminal functional groups must be independently synthesized and co-assembled.<sup>31,32</sup>

In addition to size and surface functionalization features, these supramolecular assemblies also must exhibit excellent host-guest characteristics. For example, most cancer chemotherapeutic molecules are highly toxic. Therefore, it is essential that drug molecules are stably encapsulated within the interiors of these vehicles to prevent premature release of drug molecules, when these systems undergo large dilution during biodistribution and when interacting with biological components such as cellular membranes and serum proteins that can competitively sequester these molecules to cause off-target release.<sup>33–35</sup> A consequence of stable encapsulation is that these nanoassemblies must be programmed to release their hydrophobic guest molecules in the presence of a bio-relevant trigger, such as a biomarker for a disease so that the drug molecules are released at the location of a specific lesion.<sup>12,36</sup> The intrinsic instability of the micelles under diluted conditions will cause the disassembly and premature release of the drug molecules especially under complex serum condition. Therefore, it is difficult to achieve high encapsulation stability for the block copolymer micelle.<sup>34,35,37–39</sup> For instance, the widely used PEG-PDLLA block polymer micelle has been found to rapidly release the encapsulated hydrophobic agents during circulation under *in vivo* conditions.<sup>40</sup> Even the polyethylene glycol-phospholipid micelles with enhanced stability were proposed, however, the NPs can only be stable for 1 to 2 h under serum conditions.<sup>41</sup> Even though the increased polymeric hydrophobicity of the micelle may enhance the encapsulation, the encapsulated drug would lack efficient release mechanism in these cases.<sup>34,36</sup>

Recent molecular design strategies can overcome one or more of these barriers to increase the chemotherapy efficiency.<sup>42–45</sup> For instance, layer-by-layer approaches have been used to prepare assemblies with tailorable crosslinking-based stabilization and surface functionalization features.<sup>46</sup> Similarly, shell-crosslinked micelles have been developed for enhancement of the carrier stability and facile surface engineering.<sup>47</sup> Nonetheless, fulfilling all these structural and functional requirements, mentioned above, in a single system continues to be a challenge.

Moreover, introducing functional groups in NPs often involve multiple and often tedious steps. Multi-component reactions (MCRs), involving three or more starting materials performed in one pot for the preparation of a single final product, have

<sup>1</sup>Department of Chemistry, University of Massachusetts, Amherst, MA 01003, USA

<sup>2</sup>Center for Bioactive Delivery, Institute for Applied Life Sciences, University of Massachusetts, Amherst, MA 01003, USA

<sup>3</sup>Molecular and Cellular Biology Program, University of Massachusetts, Amherst, MA 01003, USA

<sup>4</sup>Lead Contact

\*Correspondence: [thai@chem.umass.edu](mailto:thai@chem.umass.edu)  
<https://doi.org/10.1016/j.chempr.2019.09.001>

been of interest for their atom economy and efficiency.<sup>48–53</sup> MCRs were initially developed for the synthesis of small molecules and have been launched for the preparation of large libraries of molecules with the diversity and complexity that are critical for drug development and screening.<sup>51–53</sup> More recently, these strategies have been brought to bear for the synthesis of polymers with different topologies, structures, architectures, and properties.<sup>54–60</sup> However, to our knowledge, MCRs have not been exploited for the preparation of advanced nanostructures such as hierarchical polymeric assemblies with tailorable properties. In this paper, we use an efficient one-pot multi-component sequential reaction for the preparation of the complex supramolecular nanoassemblies with tunable features desired in a therapeutic delivery vehicle, where the surface functionalization and crosslinking-based stabilization of nanocarrier are achieved simultaneously in one pot with water as the solvent.

Our approach to prepare NPs and its features that highlight the key advantages in drug delivery applications include the fact that (1) the synthetic procedure is simple to perform multistep reaction for NPs in one pot, which is beneficial for scalability; (2) the reaction is performed with high atomic efficiency in a green solvent, water; (3) the NPs exhibit high encapsulation stability because of their crosslinked nature; (4) the NPs are triggerable for molecular release, as the crosslinks are based on disulfide bonds that are susceptible to the reducing intracellular conditions;<sup>61</sup> and (5) the nature of the self-assembly process and the multi-component feature allows for an unprecedented and convenient tunability in size, hydrophobicity of the interior, and surface functionalities. We elaborate the details of our preliminary findings and details in this paper.

## RESULTS AND DISCUSSION

### Three-Component Sequential Reaction for NPs with Controllable Sizes

Simple synthetic procedure to prepare the NPs, while offering the flexibility in endowing them with functional characteristics, is the key for a scalable impact. Cascade chemical reactions in a single pot offer that unique opportunity. The three-component sequential reaction that is used in the formation of the nanoassembly involves two reactions, where the reactive functionality for the second step is generated in the first step and the functional groups involved in the first and the second step are mutually compatible. The molecular design that offers this possibility is shown as P1 in Figure 1. We note here that the synthesis of the random copolymer itself requires much lower levels of synthetic efforts, compared to the block copolymer, which is good for scale up.<sup>22–24</sup> This random copolymer contains a hydrophilic poly-ethyleneglycol (PEG) methacrylate and two different hydrophobic methacrylate monomers containing an amine-reactive  $\gamma$ -thiolactone unit and a thiol-reactive pyridyldisulfide unit. In this case, an externally added amine (R-NH<sub>2</sub>) would specifically react with the  $\gamma$ -thiolactone unit to cause a ring opening of the latter to reveal a thiol moiety. This thiol moiety would then react with the pyridyldisulfide moiety to generate disulfide bonds. We hypothesized that in a polar environment, this random copolymer would self-assemble into a nanoscale structure, which can be captured using the three-component reaction induced crosslinking process. The initial amide bond formation using the substituted primary amine allows for incorporation of variations in the functional groups present within the interior of the polymer assembly, as well as on the surface of the NPs (Figure 1). The ring opening and the disulfide bond formation reactions provide the crosslinking required for the formation of the NP. Moreover, if the crosslinking process occurs exclusively within the initially formed aggregate, i.e., without any crosstalk among the nanoassemblies, then the

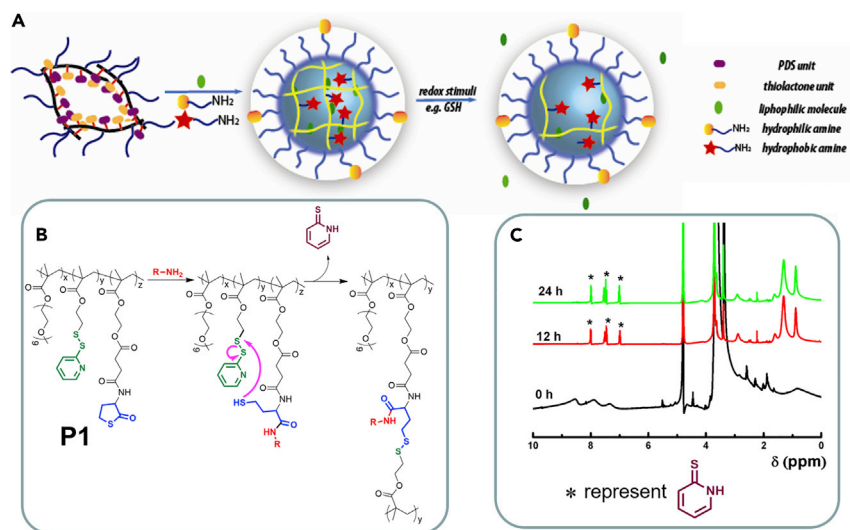


**Figure 1. Three-Component Sequential Reaction for the Preparation of the NPs**

(A) Schematic illustration of preparation of the NPs and their responsive release process.

(B) The chemical transformation of three-component sequential reaction for NPs.

(C) NMR spectra for monitoring the three-component sequential reaction process in D<sub>2</sub>O. The stars represent the byproduct (pyridinethiol) from the reaction as the readout.

ability to achieve variations in non-covalent supramolecular assemblies would directly offer access to various crosslinked NPs.

The thiolactone-containing monomer synthesis started with the reaction of DL-homocysteine thiolactone hydrochloride with succinic anhydride in the presence of sodium bicarbonate. The resultant carboxylic acid moiety was coupled to hydroxyethylmethacrylate (HEMA) monomer under 1-ethyl-3-(3-dimethylaminopropyl)carbodiimide (EDC)-coupling conditions to obtain the targeted monomer (see [Supplemental Information](#) for details). Note that the amine moiety of the starting material could indeed be directly coupled with methacrylic acid to obtain a monomer with the thiolactone on the side chain. However, the solubility of this monomer was not compatible for copolymerization with other monomers in this reaction. Polymer P1 was obtained through copolymerization of the thiolactone monomer above with PEG-methacrylate and pyridyldisulfidyl-ethyl-methacrylate monomers under RAFT polymerization conditions. To label the polymer P2, a P1 analog with a fluorophore label, these three monomers were copolymerized with a small percentage of an additional monomer containing rhodamine B. Synthetic and characterization details for the monomers and the polymers are described in [Schemes S1–S4](#) and [Figures S1–S11](#). Molecular weight ( $M_n$ ) of P1 is  $\sim 14$  k with a dispersity of 1.1. The ratio of the chemical compositions (PEG: thiolactone [TLt]: pyridyldisulfide [PDS]) was found to be about 30: 35: 35 based on the NMR integration of their characteristic peaks respectively at 3.37, 4.61, and 8.46 ppm ([Figure S7](#)). The dye labeled polymer (P2) has almost the same composition with  $\sim 1\%$  of rhodamine B label.

The next step was to use this polymer precursor to test the idea of using the three-component sequential reaction to prepare crosslinked polymeric NPs. To qualitatively assess whether the amphiphilic random copolymer forms assemblies in aqueous phase, <sup>1</sup>H NMR of P1 was assessed in D<sub>2</sub>O. Indeed, the aromatic peaks that correspond to the PDS units in the polymer were found to be very broad ([Figure 1C](#)) in relation to the same polymer in an organic solvent (see [Supplemental](#)

**Information**). This observation was taken to indicate the formation of a nanoscale aggregate in aqueous phase, where the PDS units are mostly buried within the interior of the assembly with limited segmental mobility. Upon the addition of 1 equiv of octylamine, there was a clear emergence of sharp aromatic NMR peaks that are attributed to the formation of the pyridothione byproduct of the anticipated three-component reaction.

The reaction was deemed efficient as all the PDS groups in the polymer aggregate seem to have been transformed to the pyridothione within 12 h even at low reactant concentrations. For comparison, when the same three-component reaction was also performed in an organic solvent, where no self-assembly is anticipated, the reaction was found to be much slower (Figure S18). This is understood as the hydrophobicity-driven nanoaggregate formation in water would significantly increase the local concentration of the reactively complementary moieties.

Next, we were interested in controlling the properties of the NPs, specifically their size. The ability to vary size of the NPs was motivated by the fact that the impact of nanoassemblies in many biological applications, such as drug delivery, is dictated by size.<sup>25</sup> These precise size requirements do also vary with different disease models.<sup>62</sup> Therefore, an ideal nanoscale platform would allow control over size of the NPs. To this end, we attempted to vary the self-assembly conditions that would offer variations in the size of the nanoassemblies. When P1 was assembled in water at 10 mg/mL concentration, the resultant aggregate was found to be ~15 nm at room temperature (Figure S19). When this aggregate was crosslinked at ambient temperature with hexylamine, the polymer NP was found to be ~10 nm, suggesting that the intermolecular crosslinking process could cause collapse of the aggregate (Figure 2A). We also used different amines to trigger the three-component sequential reaction for NPs under different solvents at ambient temperature. All the NPs revealed similar sizes in the range of 10–20 nm (Figure S20). We further explored the possibility of utilizing the propensity of PEG-based polymers to exhibit variations in aggregate sizes, because of their temperature-dependent dehydration possibilities.<sup>63,64</sup> Indeed, as we increased the temperature to 70°C, the size of the aggregates increased, which was also found to exhibit a systematic dependence on the concentration of the polymer. With this observation, we were able to tune the size of the NPs over a broad range from 30 nm to 40, 60, 170, or even ~1,000 nm by using polymer concentrations of 2 to 5, 10, 20, and 30 mg/mL (Figures 2 and S21), when the crosslinking reaction was carried out at 70°C.

Size of these NPs were mainly determined by dynamic light scattering (DLS), where all assemblies exhibited excellent correlation function. Although these particles were formed at 70°C, DLS measurements were performed at ~25°C, where the initial assemblies were found to be substantially smaller. The fact that the sizes of the crosslinked assemblies did not change at 70°C (Figure S21C) suggests that the crosslinking process can efficiently lock the size of the NPs. The NPs were also characterized using transmission electron microscopy (TEM), as shown in Figure 2. The NPs were spherical and exhibited a slight decrease in size, relative to that from DLS measurements, suggesting that these soft NPs collapse in dry state. Finally, it is noteworthy that all these NPs were found to be stable in water for long periods of over a month (Figure S22).

### Functionalization of the NPs

Functionalization of the NPs affords us the opportunity to tune the properties for a wide range of applications. A key feature of the three-component sequential reaction here is that the primary amine, used as the initiating reactant of the reaction cascade, offers the opportunity to incorporate diverse functionalities on the NP

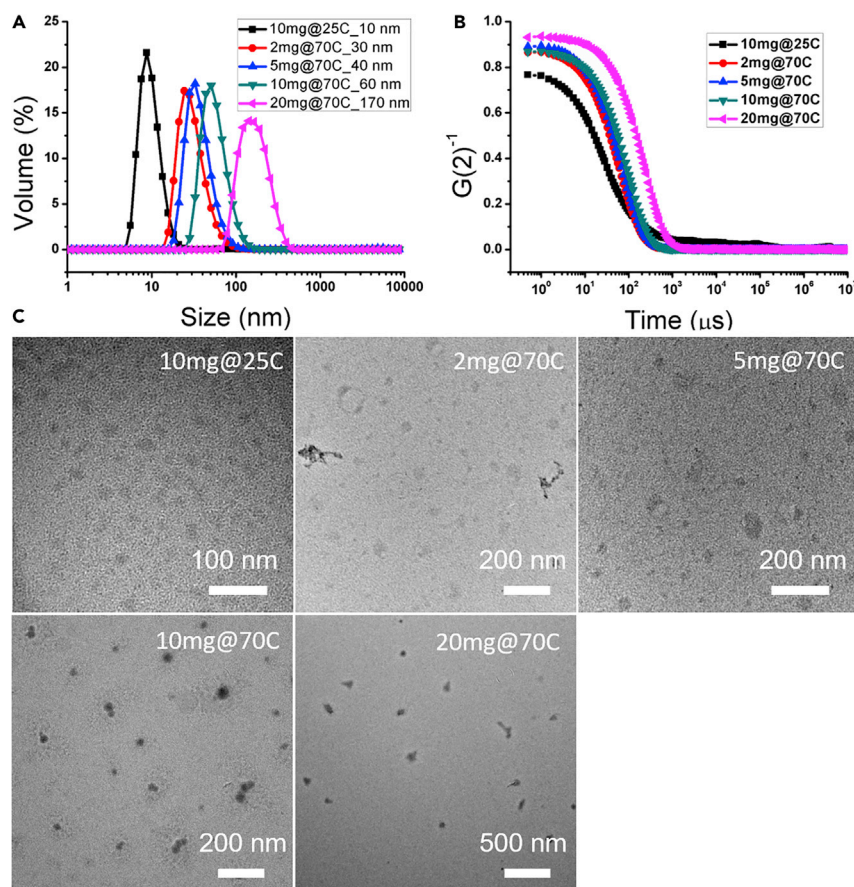


**Figure 2. Size Control of the NPs**

(A) Size of the NPs by DLS from different preparation methods (measurements were performed at 25°C). The size of the NPs was varied from 10 nm to 30, 40, 60, and 170 nm.

(B) Correlation function of the NPs from DLS. All the NPs exhibited good correlation functions.

(C) Unstained TEM images of corresponding NPs with different sizes from different preparation methods. The names represent the preparation conditions for different NPs. For example, 10mg@70C means the NPs were prepared with 10 mg polymer in 1 mL water at 70°C.

surface. To this end, we systematically varied the alkyl group in the alkylamine, R-NH<sub>2</sub>. Accordingly, we initiated the crosslinking reaction with alkyl moieties containing a negatively charged carboxylic acid moiety or a positively charged quaternary ammonium group, along with a control that does not bear any charge (hexylamine). The charged nature of the first two functionalities should dictate the surface charge of the NP, which was assessed with zeta potential measurements (Figure 3). The surface charge of the functionalized particles was indeed found to be negative (−42.8 eV) for the carboxylic-acid-functionalized NP, while the ammonium-functionalized NP exhibited a positively charged surface (+11.4 eV). Interestingly, the hexylamine-functionalized control NPs were found to be negatively charged, albeit with a lower magnitude. This observation is, however, consistent with other PEG-functionalized NPs reported in the literature.<sup>65</sup>

A reasonable expectation, among these structural variations, is that the surface exposure of the modifying functionalities would be dictated by their solvophobicity. Thus, when the modification is based on a hydrophilic functionality, these functionalities would be mostly presented on the exterior of the NP. Conversely, the

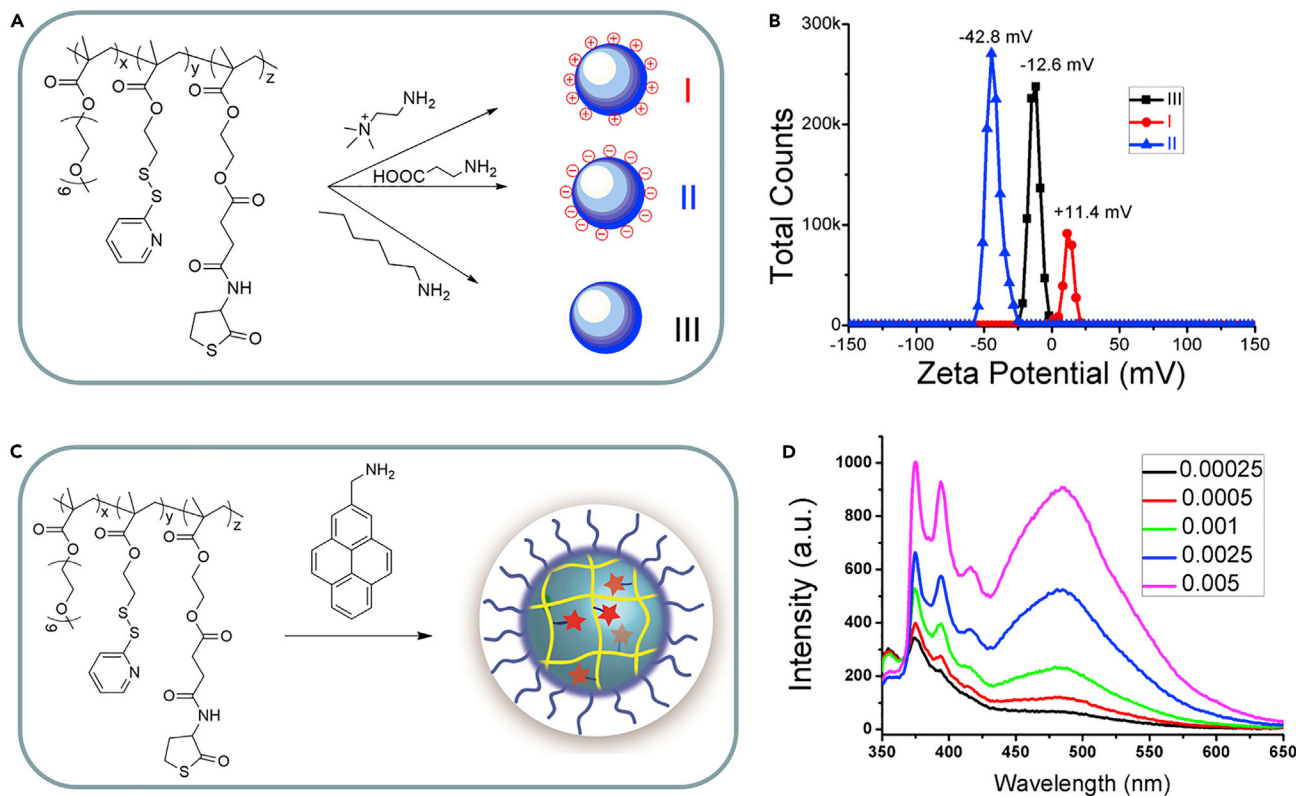


**Figure 3. Functionalization of the NPs**

(A and B) Functionalization of the NPs with different charged species on the surface: (A) chemical illustration of the functionalization and (B) zeta potential of the NPs.

(C and D) Interior functionalization: (C) chemical illustration and (D) emission spectra of the NPs with different concentrations (unit: mg/mL).

hydrophobic moieties would mainly become part of the core of the NP. While the zeta potential measurements support this hypothesis for the positively and negatively charged NPs, we further explored the hydrophobic modifications with pyrene-methylamine, a spectroscopic probe. The absorption and emission spectra of this modification are shown in Figures S23 and 3D, respectively. The characteristic absorption peak for pyrene showed the functionalization of the NP with the pyrene functionality. On the other hand, the presence of the excimer emission peak along with the monomer emission peak in the fluorescence spectrum suggests that these functionalities are most likely present within the interior of the NP. To further explore whether these excimer peaks are due to an aggregation of surface exposed pyrene moieties, the NP solution was diluted by about 20 times and the excimer emission peak could still be seen. These data further support the idea that the hydrophobic modifications mostly affect the interior of the NP. This feature has implications in the host-guest properties of these NPs, which we explored further (*vide infra*).

In order to demonstrate the utility of the facile surface functionalization capabilities, we targeted the decoration of the NPs with functionalities that can specifically target a sub-cellular compartment in a cell. Prior to carrying out any cellular experiments, it is imperative that we test whether these NPs are cytotoxic, as this might preclude any meaningful sub-cellular targeting. Accordingly, toxicity of the NPs was assessed using an MTT assay. The NPs did not exhibit any discernible cytotoxicity, even at a concentration of 0.2 mg/mL (Figure 4A). The data shown in Figure 4A are based on 60 nm NPs. To assess whether size variations have any effect on the cytotoxicity,

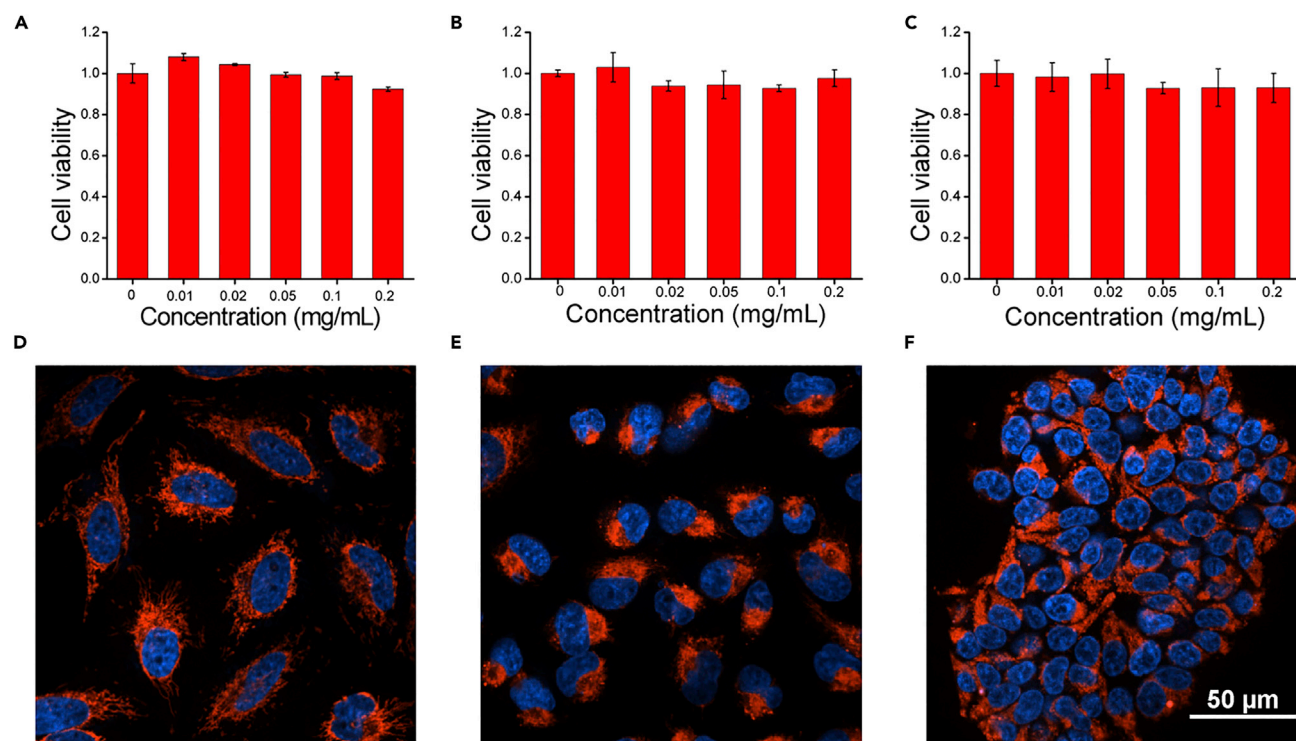


**Figure 4. Cytotoxicity and Cell Uptake of the NPs**

Cytotoxicity (A–C) and cell uptake (D–F) of the NPs (size: 60 nm) in (A and D) HeLa cells, (B and E) MDA-MB-231 cells, and (C and F) MCF-7 cells. The cytotoxicity was performed by MTT assay. The confocal images were recorded after 4 h incubation with the concentration of 30  $\mu\text{g}/\text{mL}$  of NPs. The red color represents the rhodamine-B-dye-labelled NGs. The blue color represents the nucleus after hoechst 33342 staining.

NPs of different sizes were assessed and were also found to be non-toxic (Figure S25). To even further test these NPs, the cytotoxicity of the 60 nm NPs was also studied in two more cell lines, MDA-MB-231 and MCF-7 (Figures 4B and 4C). Here too, the NPs were found to be quite cyto-compatible. A potential issue with a typical cytotoxicity analysis is that a NP might be deemed non-toxic, because it never was taken up by the cell and thus does not induce any toxicity. To test this possibility, we tested whether the NPs are taken up by the cells using rhodamine-B-labeled NPs (Figures 4D, 4F, and S26–S28). The presence of the bright red color, from the covalently attached rhodamine B, throughout the cells indicates that these NPs are taken up by the cells after a short incubation time of 4 h. This feature too was found to be true for MDA-MB231 and MCF-7 cell lines (Figures 4E and 4F) and for NPs of different sizes (Figures S27 and S28).

To investigate the possibility of sub-cellular targeting using functionalities presented on the surface of the polymer NPs, triphenylalkylphosphonium moieties were incorporated on the surface of the NPs, as these functionalities are known to target mitochondria. Structure of the polymeric NP is shown in Figure 5. Synthetic and characterization details of the ligand molecules and their incorporation on the surface of the NPs are detailed in Scheme S5 and Figures S12–S17. The intracellular distribution of the NPs and the potential mitochondrial targeting was studied using a high-resolution confocal microscope. In this experiment, the mitochondria were stained with a green mito-tracker dye. NP localization in the mitochondria was then assessed by evaluating the colocalization of the green color from this dye with the red color of the rhodamine-labeled NP. As shown in Figure 5, the triphenylalkylphosphonium-decorated NPs exhibited excellent mitochondrial localization, while the unfunctionalized NP exhibited

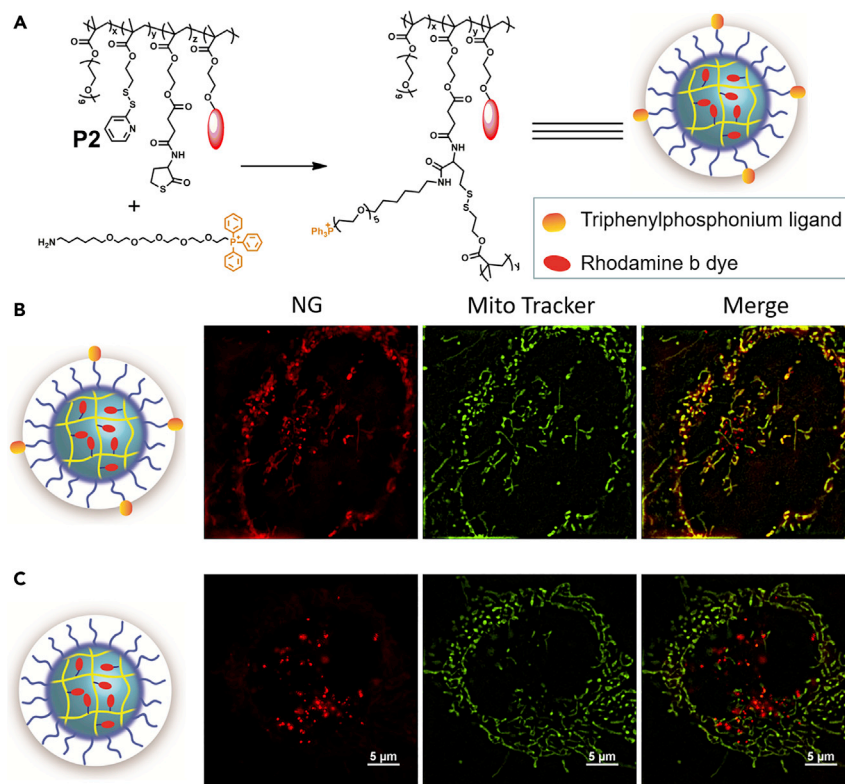


**Figure 5. Mitochondria Targeting Experiment**

(A) Schematic illustration of the preparation of ligand-functionalized NPs.

(B and C) The resonant scanning confocal with structured illumination super-resolution (SIMe) images of NP uptake by HeLa cell after 4 h incubation for (B) ligand-functionalized NPs and (C) control NPs without ligand.

no localization in the mitochondria (Figures 5B and 5C). The ability to deliver NPs to specific sub-cellular organelle offers many opportunities for improving therapeutic approaches through targeting.<sup>66</sup>

### Non-covalent Encapsulation and Triggered Release of Guest Molecules

Stable encapsulation of the guest molecules with a triggerable release modality is the key feature to ultimately implement these NPs in practical applications. In addition to the surface functionalization, we also surmised that when modified with hydrophobic amines, the interior of these NPs would be affected. To test this idea further, we tested the non-covalent encapsulation capability of the NPs. Accordingly, we systematically varied the hydrophobicity of the modifying functionality in the NP using hexylamine, octylamine, decylamine, and benzylamine. The ability of these NPs to non-covalently bind to guest molecules was assessed using Nile red as the probe. All NPs exhibited the ability to non-covalently bind the spectroscopic probe, where the extent of guest loading inside the NPs seemed to depend on the functional group. Interestingly, octylamine-modified NPs exhibit an optimal ability to bind Nile red, compared to both hexylamine and decylamine (Figure S24). These results could be rationalized by the possibility that there is a balance between the hydrophobicity of the modifying functionality and its sterics-induced volume exclusion.

An equally important criterion for a good host, especially in the context of a drug carrier, involves the encapsulation stability of the guest molecule in the NP. The

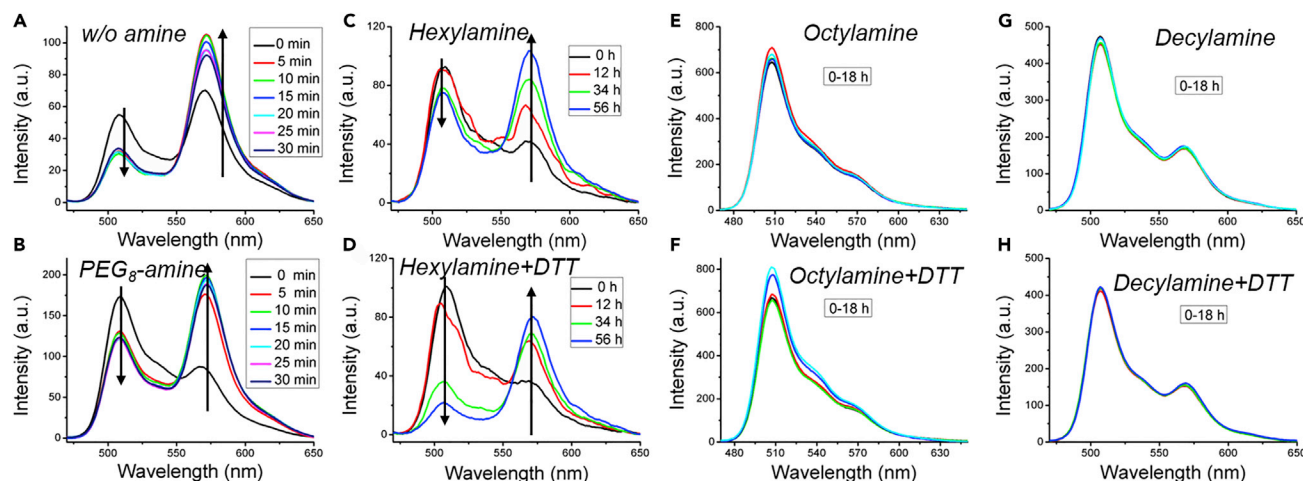


**Figure 6. FRET Experiment of NPs from Different Amines**

(A) No amine.

(B) PEG<sub>8</sub>-amine.

(C and D) Hexylamine.

(E and F) Octylamine.

(G and H) Decylamine.

(A–C, E, and G) In the absence of DTT.

(D, F, and H) In the presence of 10 mM DTT.

The fluorescent spectra were measured by excitation wavelength at 450 nm.

encapsulation stability of the NP for hydrophobic guest molecules should directly correlate with the hydrophobicity of the modifying amine functionality. We used the previously developed fluorescence resonance energy transfer (FRET)-based method<sup>67</sup> to evaluate the encapsulation stability of the NPs. In brief, a solution containing a FRET donor molecule as the guest in the NP host is mixed with a similar solution with the corresponding FRET acceptor molecule as the guest. The kinetics of FRET evolution provides direct insights into the encapsulation stability; faster FRET evolution indicates poor encapsulation stability.

Hydrophobic cyanine dyes, DiO and DiI, were used as the FRET donor and acceptor molecules, respectively, for this study. First, the encapsulation stability of the amphiphilic polymer assembly, before crosslinking, was assessed as the control. The non-crosslinked polymeric nanoaggregate showed very fast FRET increase rate with a rapid increase of the acceptor emission at 550 nm and decrease of the donor emission at 510 nm (Figure 6A), with a leakage coefficient of >18/h, suggesting a leaky nanoaggregate. Next, the crosslinked NPs based on the reaction with hexylamine was evaluated. Here too, there was a temporal evolution of the FRET ratio; however, the evolution was found to be much slower with a leakage coefficient of  $4.57 \times 10^{-3}$ /h (Figures 6C and S29). As the hydrophobicity of the amine increases from the hexylamine to octylamine and decylamine-based NPs, the encapsulation stability substantially increased with no discernible temporal evolution of FRET for the latter two NPs (Figures 6E and 6G). The alkylamine-induced crosslinking reaction can provide enhanced encapsulation stability due to two different reasons—enhanced hydrophobicity of the interior endowed by the incorporation of the alkyl moiety and the crosslinking of the interior that offers increased steric barrier for molecular diffusion out of the NPs. The increased encapsulation stability with increasing hydrophobicity of the alkyl chain suggests that the former is certainly a factor. To test whether there is contribution from the latter, the NP crosslinking

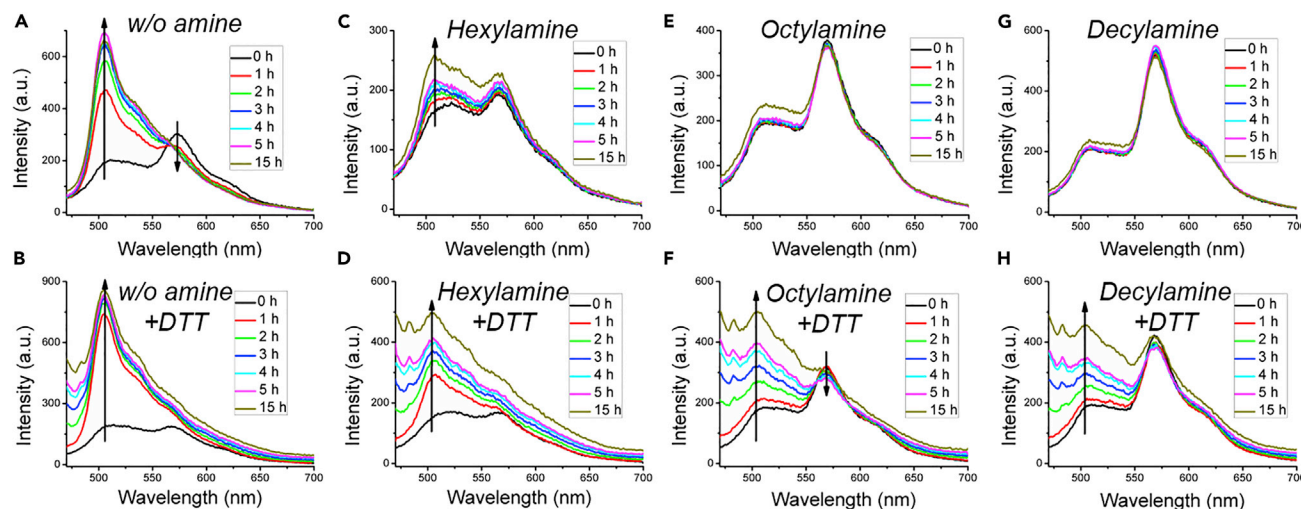


**Figure 7. Serum Stability Test toward NPs Prepared from Different Amines**

All the FRET experiments were performed in serum (90%).

(A and B) No amine.

(C and D) Hexylamine.

(E and F) Octylamine.

(G and H) Decylamine.

(A, C, E, and G) In the absence of DTT.

(B, D, F, and H) In the presence of 10 mM DTT.

The fluorescent spectra were measured by excitation wavelength at 450 nm.

was initiated using a hydrophilic polyethyleneglycol-amine (PEG<sub>8</sub>-amine). The resultant NP exhibited better encapsulation stability, compared to the uncrosslinked control nanoaggregate, with a leakage coefficient of  $\sim 4.2/h$ . However, this encapsulation is much poorer compared to that from the hexylamine. These results clearly show that both crosslinking-based steric barrier and hydrophobicity-based encapsulation play critical roles in the encapsulation stability of these NPs.

If these NPs were to be useful, it is also essential that this stable encapsulation is compromised in the presence of a specific biologically relevant trigger. Because of the presence of the disulfide bonds, these are likely to be susceptible to the presence of a reducing agent such as dithiothreitol (DTT). Indeed, the FRET evolution was found to be significantly faster in the presence of mM concentration of DTT (Figures 6D and S30). Interestingly, however, no change in FRET evolution was observed for octylamine- and decylamine-based NPs even in the presence of DTT (Figures 6F and 6H). The main reason is the increase in the hydrophobicity to stabilize the NPs under pure water solution. When we use serum as the medium (*vide infra*), the dye can still be released out from the NPs in the presence of DTT. Based on the results, we conclude that crosslinking can efficiently enhance the stability of the NPs.

The studies above show that the encapsulation stability in these NPs is dependent on the hydrophobicity of the modifying functionalities and the crosslinks in the NP in aqueous solution. An even more rigorous study of the encapsulation stability in the context of biological applications would involve evaluating it under serum conditions. We adapted a previously reported method<sup>68</sup> for this purpose, where the FRET pairs are co-encapsulated in the NP. In this case, the solution already exhibits excellent FRET (Figure S31). If the encapsulation stability is poor, the hydrophobic guests would leave the interior of the NP and accumulate in the reservoir offered by the serum proteins that are capable of binding to hydrophobic molecules,

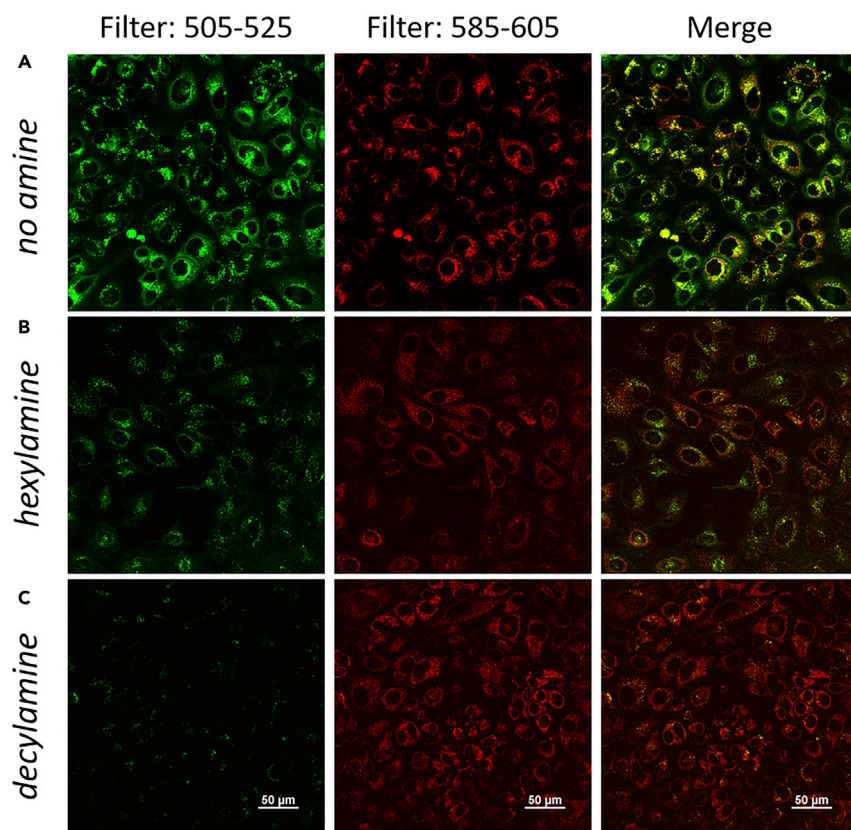


**Figure 8. In-Cell FRET Experiment toward Different NPs from Different Amines**

(A) No amine.

(B) Hexylamine.

(C) Decylamine inside cells (HeLa cell line) after 24 h incubation.

The confocal images were recorded by excitation wavelength of 488 nm, and the images were obtained with two different filters in the ranges of 505–525 and 585–605 nm.

such as serum albumin. Interestingly, the leakage coefficient of the uncrosslinked nanoaggregates and the hexylamine-based NPs was found to be higher in serum (Figure 7). Here too, the octyl- and the decyl-NPs were still found to exhibit stable encapsulation. However, when the experiments were performed in the presence of 10 mM DTT, even the octylamine- and decylamine-based NPs exhibited a lower FRET ratio over time, as discerned by the increase of the donor peak and decrease of the acceptor emission peak (Figures 7F and 7H). These results also show that our strategy can efficiently endow the particles with high encapsulation stability without any leakage of the guest molecules under serum conditions. On the other hand, there have been recent reports that show that micelles based on many block copolymers can stably encapsulate hydrophobic molecules in water but exhibit fast leakage under serum conditions at the time scales used in the present work.<sup>38–41</sup> These results also highlight that encapsulation stability in water is not a sufficient measure for evaluating NPs for biological applications such as targeted drug delivery.

Next, we evaluated whether the observed trend in encapsulation stability translated to molecular release kinetics variations inside cells, as the cytosolic environments of most cells are highly reducing. If we were to use the encapsulated FRET pairs, we might not be able to discern the difference between cellular uptake

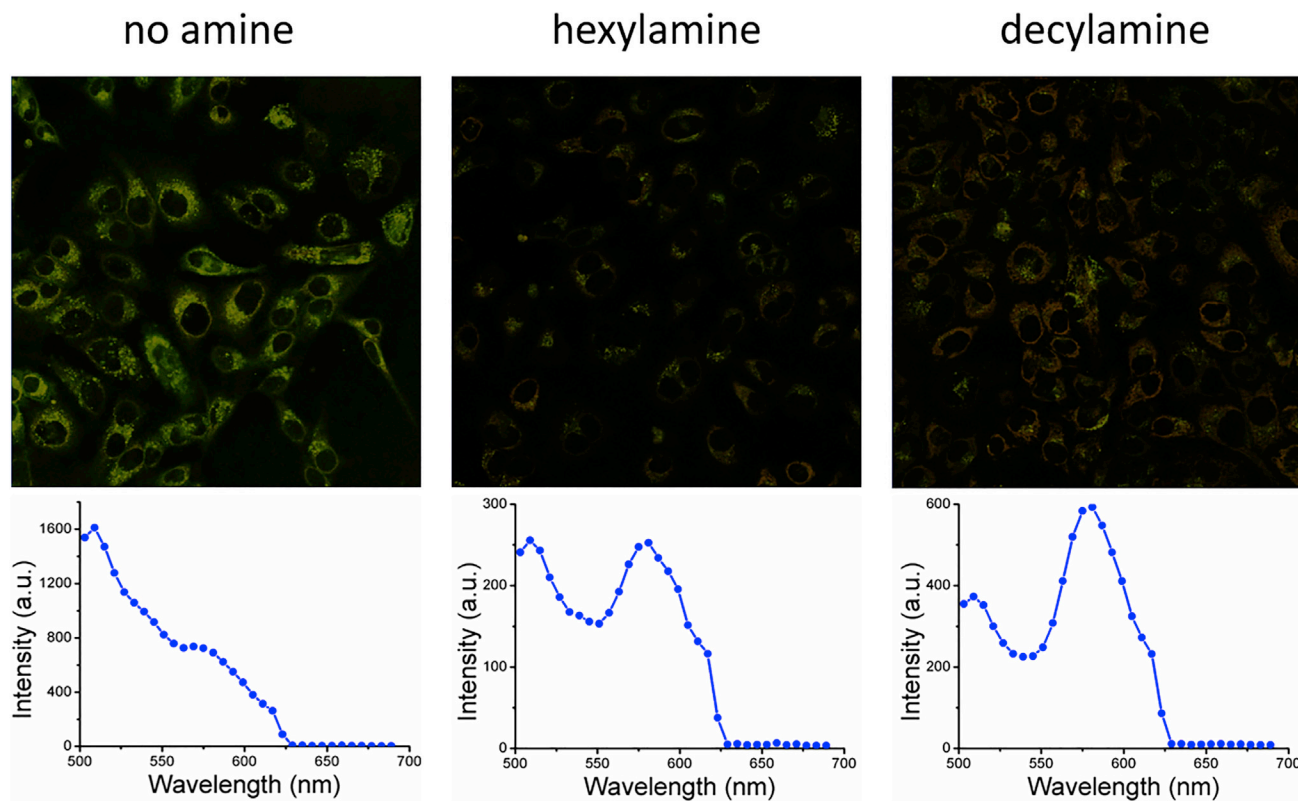


**Figure 9. In-Cell FRET Study of Different NPs from Different Amines (No Amine, Hexylamine, and Decylamine)**

The images and spectra were obtained from the spectral confocal microscope with excitation wavelength at 488 nm after 24 h incubation.

followed by molecular release and leakage of molecules outside the cells where the hydrophobic molecules can then passively diffuse inside the cells. To circumvent this, the NPs were covalently labeled with rhodamine B, which can act as the FRET acceptor for the donor dye DiO. The latter was non-covalently encapsulated as the hydrophobic guest molecules within the NPs (Figure S32). The principle of this method is similar to the experiments in the serum, where there would be a high FRET because of the concurrent presence of both the donor and the acceptor in the NP. However, if the non-covalently encapsulated molecules were to be released, then the decreased proximity between these molecules will substantially impact the FRET. We used the spin disk fluorescent microscope and A1R spectral microscope to study the encapsulation stability in HeLa cells after 4 and 24 h incubation times. As the donor DiO is a green dye, we used the 488 nm laser for excitation. Two different filters were monitored for emission: the 505–525 nm channel present the DiO emission and the 585–605 nm channel present the rhodamine B acceptor emission (Figures S33 and 8). The relative intensity of the green channel and the red channel, which also dictates the color in the merged channel, provides insights into the relative kinetics of molecular release from the NPs. For the non-crosslinked nanoaggregate, there is a significant emission from the green channel and the merged image is quite green, suggesting that the DiO guest molecule has been released from the NP. The hexylamine-based NP shows a mixture of the green and red fluorescence in the merged image indicating slow release of the guest molecule, while the domination of the red fluorescence in the decylamine NP suggests high encapsulation stability with very little to no molecular release in 24 h.

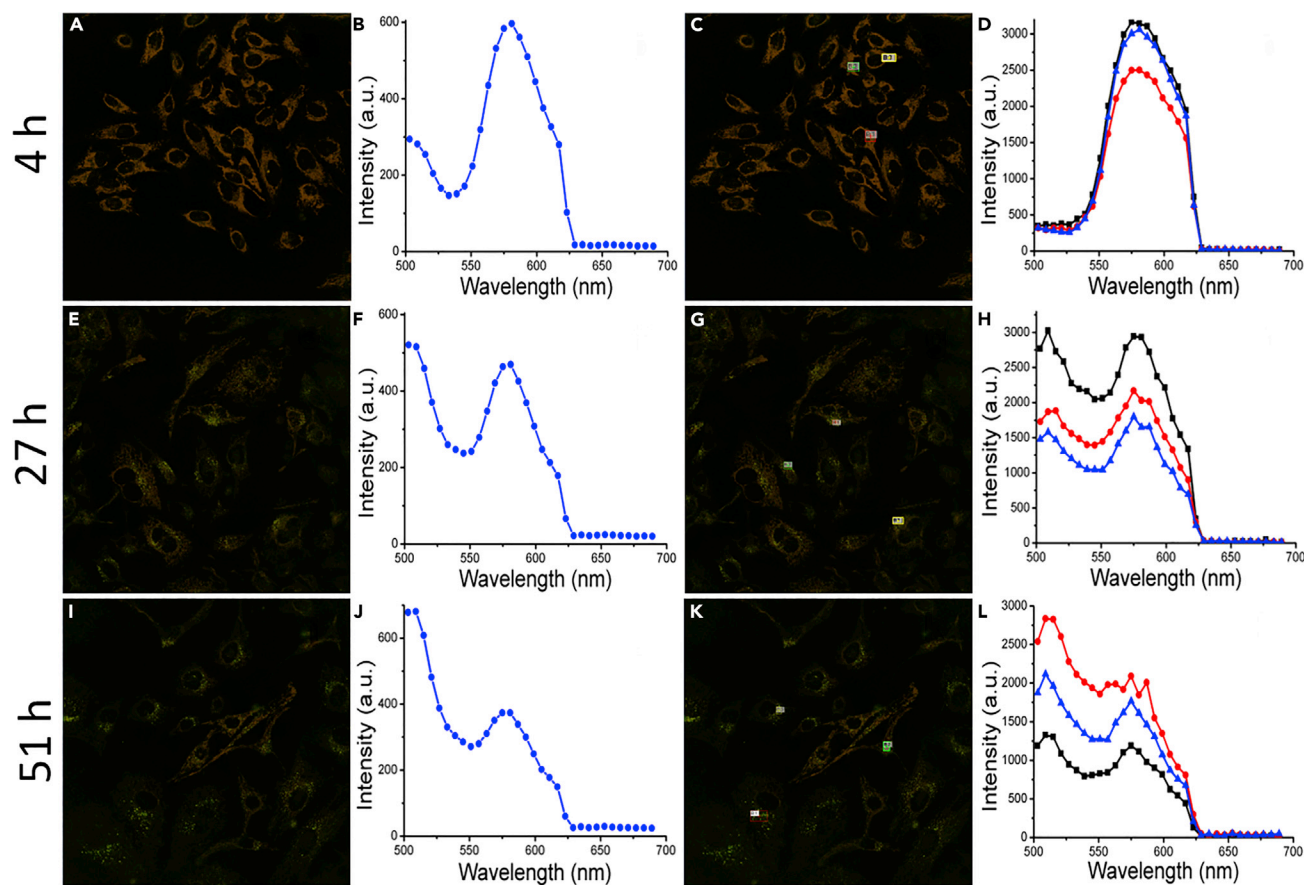


**Figure 10. Time-Dependent In-Cell FRET Study of NPs (from Hexylamine)**

The images and spectra were obtained from the spectral confocal microscope with excitation wavelength at 488 nm after different time incubation (4, 27, and 51 h).

(A, E, F, C, G, and K) Spectral images.

(B, F, and J) Emission spectra from (A), (E), and (I), respectively.

(D, H, and L) Emission spectra from the selected areas in (C), (G), and (K), respectively.

To more quantitatively compare the encapsulation stability inside cells, we used spectral confocal microscope to obtain the emission spectra inside the cells. Three different nanocarriers (non-crosslinked nanoaggregate, hexylamine-functionalized NPs, and decylamine functionalized NPs) were studied by cell uptake after 24 h incubation (Figure 9). There is very little FRET in the cells (FRET ratio  $I_a/(I_a + I_d) = 0.26$ ) for non-crosslinked nanoaggregates, which is attributed to the possible release of the guest molecules even prior to cellular uptake. After the hydrophobic functionalization of the NPs with hexylamine to decylamine, the FRET ratios were found to be much higher with values of 0.49 and 0.62.

To further assess whether there is a time-dependent intracellular release of the guest molecules, the FRET ratio was monitored for the hexylamine-based NPs at 4, 27, and 51 h. As shown in Figure 10, the emission at  $\sim 560$  nm decreased, with a concurrent increase in the emission at  $\sim 510$  nm. This change corresponded to the FRET ratios 0.68, 0.47, and 0.33 at 4, 27, and 51 h, respectively. Moreover, the site-selected spectra obtained from inside the cells also showed similar results (Figures 10D, 10H, and 10L). These results clearly show that the intracellular reducing environment of the cells, due to high glutathione concentration, can cause molecular release

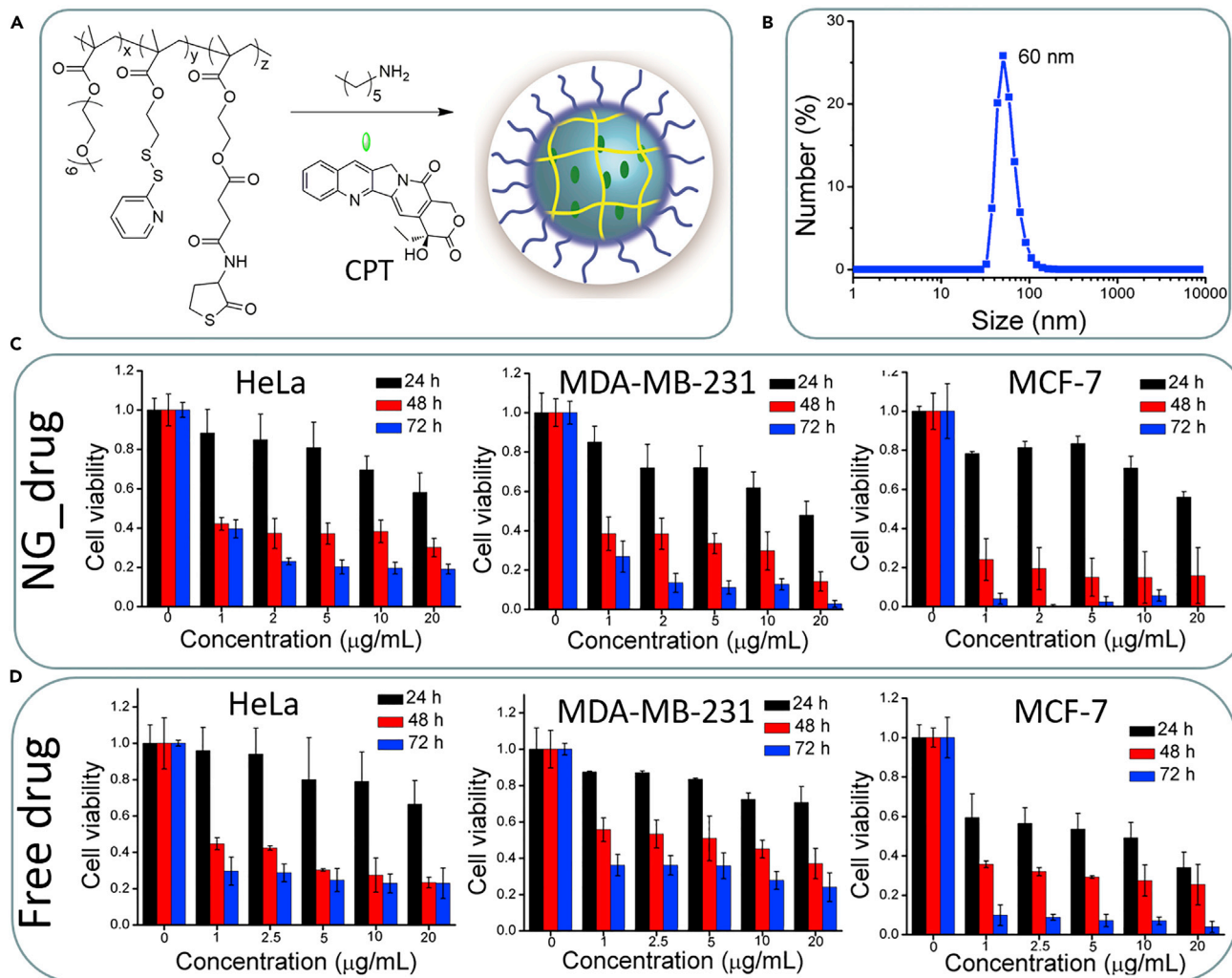


**Figure 11. Cytotoxicity of the Drug-Loaded NPs**

(A) Schematic illustration for the preparation of drug (CPT)-loaded NPs.

(B) DLS of CPT-loaded NPs.

(C) Concentration and time-dependent cytotoxicity of the drug-loaded NPs.

(D) Cytotoxicity of the free drug.

inside cells, the rate of which is correlated with the encapsulation stability obtained in test tube experiments.

As the NPs exhibit many tunable features that are translatable inside cells, we carried out preliminary experiments to assess the possibility of these NPs acting as a carrier for chemotherapeutic drug molecules to be released under intracellular conditions. We used camptothecin (CPT) because of its hydrophobicity and well-established pharmacology. A ~60 nm hexylamine-based NP was synthesized with 13% loading capacity (1.3 mg drug/10 mg polymer) of the drug (Figures 11B and S34). Cell viabilities were then evaluated at different concentrations of CPT-loaded NPs in three different cancer cells (HeLa, MDA-MB-231, and MCF-7). The extent of cell death was investigated after different times (24 h, 48 h, and 72 h). The cell death efficiency was comparable with free drug in most cases for the NP and was even better in some cases suggesting that the NP is capable of making the hydrophobic drug molecules more bioavailable.

## Conclusions

A facile strategy for the preparation of NPs with tailorable properties through concurrent functionalization and stabilization has been demonstrated using a sequential three-component reaction. By tuning the polymeric structure and self-assembly conditions, we have shown that the non-covalent assembly and thus the resultant NP sizes can be conveniently tuned by 2 orders of magnitude. Similarly, the functionalization of the NPs can be used to decorate the outer shell of the NP to tune its interfacial interaction or to functionalize the interior to optimize its host-guest properties. The former feature has been used to vary the surface charge of the NPs and to target specific organelles in cells. The latter option has been exploited to evaluate variations in the hydrophobicity that offer an optimal encapsulation stability, where the guest molecules are robustly encapsulated in one set of conditions but are reliably released in a target environment. Three different FRET-based methods, including an in-cell FRET experiment, have been used to test the effect of core structure variations upon encapsulation stability in aqueous solutions, in serum, and inside cells. The ability to tightly tune the physiochemical properties of NPs has implications in a variety of applications, including in drug delivery and diagnostics. As a preliminary demonstration, we have shown that these NPs can encapsulate hydrophobic drug molecules and can be released in the target intracellular environment with high fidelity.

## EXPERIMENTAL PROCEDURES

Full experimental procedures are provided in the [Supplemental Information](#).

## SUPPLEMENTAL INFORMATION

Supplemental Information can be found online at <https://doi.org/10.1016/j.chempr.2019.09.001>.

## ACKNOWLEDGMENTS

We thank the United States National Science Foundation (CHE-1307118) for support.

## AUTHOR CONTRIBUTIONS

B.L. and S.T. designed this project. B.L. performed the experiments. B.L. and S.T. wrote the manuscript.

## DECLARATION OF INTERESTS

The authors declare no competing interests.

Received: May 3, 2019

Revised: June 25, 2019

Accepted: September 10, 2019

Published: October 14, 2019

## REFERENCES AND NOTES

1. Mura, S., Nicolas, J., and Couvreur, P. (2013). Stimuli-responsive nanocarriers for drug delivery. *Nat. Mater.* 12, 991–1003.
2. Pelaz, B., Alexiou, C., Alvarez-Puebla, R.A., Alves, F., Andrews, A.M., Ashraf, S., Balogh, L.P., Ballerini, L., Bestetti, A., Brendel, C., et al. (2017). Diverse applications of nanomedicine. *ACS Nano* 11, 2313–2381.
3. Kumari, P., Ghosh, B., and Biswas, S. (2016). Nanocarriers for cancer-targeted drug delivery. *J. Drug Target* 24, 179–191.
4. Comoglu, T., Arisoy, S., and Akkus, Z.B. (2017). Nanocarriers for effective brain drug delivery. *Curr. Top. Med. Chem.* 17, 1490–1506.
5. Sun, T., Zhang, Y.S., Pang, B., Hyun, D.C., Yang, M., and Xia, Y. (2014). Engineered nanoparticles for drug delivery in cancer therapy. *Angew. Chem. Int. Ed. Engl.* 53, 12320–12364.
6. Liong, M., Lu, J., Kovochich, M., Xia, T., Ruehm, S.G., Nel, A.E., Tamanoi, F., and Zink, J.I. (2008). Multifunctional inorganic nanoparticles for imaging, targeting, and drug delivery. *ACS Nano* 2, 889–896.
7. Zhao, M., Zeng, E., and Zhu, B. (2015). The biological applications of inorganic

- nanoparticle drug carriers. *ChemNanoMat* 1, 82–91.
8. Pattni, B.S., Chupin, V.V., and Torchilin, V.P. (2015). New developments in liposomal drug delivery. *Chem. Rev.* 115, 10938–10966.
  9. Madaan, K., Kumar, S., Poonia, N., Lather, V., and Pandita, D. (2014). Dendrimers in drug delivery and targeting: drug-dendrimer interactions and toxicity issues. *J. Pharm. Bioallied Sci.* 6, 139–150.
  10. Uhrich, K.E., Cannizzaro, S.M., Langer, R.S., and Shakesheff, K.M. (1999). Polymeric systems for controlled drug release. *Chem. Rev.* 99, 3181–3198.
  11. Li, Y., Maciel, D., Rodrigues, J., Shi, X., and Tomás, H. (2015). Biodegradable polymer nanogels for drug/nucleic acid delivery. *Chem. Rev.* 115, 8564–8608.
  12. Kamaly, N., Yameen, B., Wu, J., and Farokhzad, O.C. (2016). Degradable controlled-release polymers and polymeric nanoparticles: mechanisms of controlling drug release. *Chem. Rev.* 116, 2602–2663.
  13. Elsabahy, M., Heo, G.S., Lim, S.M., Sun, G., and Wooley, K.L. (2015). Polymeric nanostructures for imaging and therapy. *Chem. Rev.* 115, 10967–11011.
  14. Kakkar, A., Traverso, G., Farokhzad, O.C., Weissleder, R., and Langer, R. (2017). Evolution of macromolecular complexity in drug delivery systems. *Nat. Chem. Rev.* 1, 1–17.
  15. Li, Y., Wang, Y., Huang, G., and Gao, J. (2018). Cooperativity principles in self-assembled nanomedicine. *Chem. Rev.* 118, 5359–5391.
  16. Webber, M.J., and Langer, R. (2017). Drug delivery by supramolecular design. *Chem. Soc. Rev.* 46, 6600–6620.
  17. Tibbitt, M.W., Dahlman, J.E., and Langer, R. (2016). Emerging frontiers in drug delivery. *J. Am. Chem. Soc.* 138, 704–717.
  18. Blanco, E., Shen, H., and Ferrari, M. (2015). Principles of nanoparticle design for overcoming biological barriers to drug delivery. *Nat. Biotechnol.* 33, 941–951.
  19. von Roemeling, C., Jiang, W., Chan, C.K., Weissman, I.L., and Kim, B.Y.S. (2017). Breaking down the barriers to precision cancer nanomedicine. *Trends Biotechnol.* 35, 159–171.
  20. Chen, H., Zhang, W., Zhu, G., Xie, J., and Chen, X. (2017). Rethinking cancer nanotheranostics. *Nat. Rev. Mater.* 2, 17024.
  21. Zhang, X., Jackson, J.K., and Burt, H.M. (1996). Development of amphiphilic diblock copolymers as micellar carriers of Taxol. *Int. J. Pharm.* 132, 195–206.
  22. Yokoyama, M. (2010). Polymeric micelles as a new drug carrier system and their required considerations for clinical trials. *Expert Opin. Drug Deliv.* 7, 145–158.
  23. Gaucher, G., Dufresne, M.H., Sant, V.P., Kang, N., Maysinger, D., and Leroux, J.C. (2005). Block copolymer micelles: preparation, characterization and application in drug delivery. *J. Control. Release* 109, 169–188.
  24. Cabral, H., Miyata, K., Osada, K., and Kataoka, K. (2018). Block copolymer micelles in nanomedicine applications. *Chem. Rev.* 118, 6844–6892.
  25. Torchilin, V. (2011). Tumor delivery of macromolecular drugs based on the EPR effect. *Adv. Drug Deliv. Rev.* 63, 131–135.
  26. Waku, T., Matsusaki, M., Kaneko, T., and Akashi, M. (2007). PEG brush peptide nanospheres with stealth properties and chemical functionality. *Macromolecules* 40, 6385–6392.
  27. Srinivasarao, M., and Low, P.S. (2017). Ligand-targeted drug delivery. *Chem. Rev.* 117, 12133–12164.
  28. Zhulina, E.B., and Borisov, O.V. (2012). Theory of block polymer micelles: recent advances and current challenges. *Macromolecules* 45, 4429–4440.
  29. Milchev, A., Bhattacharya, A., and Binder, K. (2001). Formation of block copolymer micelles in solution: a Monte Carlo study of chain length dependence. *Macromolecules* 34, 1881–1893.
  30. Chang, T., Lord, M.S., Bergmann, B., Macmillan, A., and Stenzel, M.H. (2014). Size effects of self-assembled block copolymer spherical micelles and vesicles on cellular uptake in human colon carcinoma cells. *J. Mater. Chem. B* 2, 2883–2891.
  31. Hisey, B., Ragogna, P.J., and Gillies, E.R. (2017). Phosphonium-functionalized polymer micelles with intrinsic antibacterial activity. *Biomacromolecules* 18, 914–923.
  32. Licciardi, M., Giammona, G., Du, J., Armes, S.P., Tang, Y., and Lewis, A.L. (2006). New folate-functionalized biocompatible block copolymer micelles as potential anti-cancer drug delivery systems. *Polymer* 47, 2946–2955.
  33. Miller, T., Breyer, S., van Colen, G., Mier, W., Haberkorn, U., Geissler, S., Voss, S., Weigandt, M., and Goepferich, A. (2013). Premature drug release of polymeric micelles and its effects on tumor targeting. *Int. J. Pharm.* 445, 117–124.
  34. Owen, S.C., Chan, D.P.Y., and Shoichet, M.S. (2012). Polymeric micelle stability. *Nano Today* 7, 53–65.
  35. Kim, S., Shi, Y., Kim, J.Y., Park, K., and Cheng, J.X. (2010). Overcoming the barriers in micellar drug delivery: loading efficiency, *in vivo* stability, and micelle-cell interaction. *Expert Opin. Drug Deliv.* 7, 49–62.
  36. Wong, P.T., and Choi, S.K. (2015). Mechanisms of drug release in nanotherapeutic delivery systems. *Chem. Rev.* 115, 3388–3432.
  37. Zou, P., Chen, H., Paholak, H.J., and Sun, D. (2013). Noninvasive fluorescence resonance energy transfer imaging of *in vivo* premature drug release from polymeric nanoparticles. *Mol. Pharm.* 10, 4185–4194.
  38. Lu, J., Owen, S.C., and Shoichet, M.S. (2011). Stability of self-assembled polymeric micelles in serum. *Macromolecules* 44, 6002–6008.
  39. Savić, R., Azzam, T., Eisenberg, A., and Maysinger, D. (2006). Assessment of the integrity of poly(caprolactone)-*b*-poly(ethylene oxide) Micelles under biological conditions: a fluorogenic-based approach. *Langmuir* 22, 3570–3578.
  40. Chen, H., Kim, S., He, W., Wang, H., Low, P.S., Park, K., and Cheng, J.X. (2008). Fast release of lipophilic agents from circulating PEG-PDLLA micelles revealed by *in vivo* Förster resonance energy transfer imaging. *Langmuir* 24, 5213–5217.
  41. Diezi, T.A., Bae, Y., and Kwon, G.S. (2010). Enhanced stability of PEG-block-poly(N-hexyl stearate *l*-aspartamide) micelles in the presence of serum proteins. *Mol. Pharm.* 7, 1355–1360.
  42. Zhang, X., Malhotra, S., Molina, M., and Haag, R. (2015). Micro- and nanogels with labile crosslinks from synthesis to biomedical applications. *Chem. Soc. Rev.* 44, 1948–1973.
  43. Dai, Y., Chen, X., and Zhang, X. (2018). Recent developments in the area of click-crosslinked nanocarriers for drug delivery. *Macromol. Rapid Commun.* 1800541.
  44. Liu, B., and Thayumanavan, S. (2017). Substituent effects on the pH sensitivity of acetals and ketals and their correlation with encapsulation stability in polymeric nanogels. *J. Am. Chem. Soc.* 139, 2306–2317.
  45. Ryu, J.H., Chacko, R.T., Jiwpanich, S., Bickerton, S., Babu, R.P., and Thayumanavan, S. (2010). Self-cross-linked polymer nanogels: a versatile nanoscopic drug delivery platform. *J. Am. Chem. Soc.* 132, 17227–17235.
  46. Kamphuis, M.M.J., Johnston, A.P.R., Such, G.K., Dam, H.H., Evans, R.A., Scott, A.M., Nice, E.C., Heath, J.K., and Caruso, F. (2010). Targeting of cancer cells using click-functionalized polymer capsules. *J. Am. Chem. Soc.* 132, 15881–15883.
  47. Joralemon, M.J., O'Reilly, R.K., Hawker, C.J., and Wooley, K.L. (2005). Shell click-crosslinked (SCC) nanoparticles: a new methodology for synthesis and orthogonal functionalization. *J. Am. Chem. Soc.* 127, 16892–16899.
  48. Espeel, P., Goethals, F., and Du Prez, F.E.D. (2011). One-pot multistep reactions based on thiolactones: extending the realm of thiol-ene chemistry in polymer synthesis. *J. Am. Chem. Soc.* 133, 1678–1681.
  49. Lundberg, P., Hawker, C.J., Hult, A., and Malkoch, M. (2008). Click assisted one-pot multi-step reactions in polymer science: accelerated synthetic protocols. *Macromol. Rapid Commun.* 29, 998–1015.
  50. Dömling, A., Wang, W., and Wang, K. (2012). Chemistry and biology of multicomponent reactions. *Chem. Rev.* 112, 3083–3135.
  51. Rotstein, B.H., Zaretsky, S., Rai, V., and Yudin, A.K. (2014). Small heterocycles in multicomponent reactions. *Chem. Rev.* 114, 8323–8359.
  52. Touré, B.B., and Hall, D.G. (2009). Natural product synthesis using multicomponent reaction strategies. *Chem. Rev.* 109, 4439–4486.
  53. Wessjohann, L.A., Rivera, D.G., and Vercillo, O.E. (2009). Multiple multicomponent macrocyclizations (MiBs): a strategic development toward macrocycle diversity. *Chem. Rev.* 109, 796–814.

54. Kreyc, O., Tóth, T., and Meier, M.A.R. (2011). Introducing multicomponent reactions to polymer science: Passerini reactions of renewable monomers. *J. Am. Chem. Soc.* *133*, 1790–1792.
55. Solleder, S.C., and Meier, M.A.R. (2014). Sequence control in polymer chemistry through the Passerini three-component reaction. *Angew. Chem. Int. Ed. Engl.* *53*, 711–714.
56. Kakuchi, R., and Theato, P. (2013). Three-component reactions for post-polymerization modifications. *ACS Macro Lett.* *2*, 419–422.
57. Deng, X., Du, F., and Li, Z. (2014). Combination of orthogonal ABB and ABC multicomponent reactions toward efficient divergent synthesis of dendrimers with structural diversity. *ACS Macro Lett.* *3*, 667–670.
58. Deng, X., Cui, Y., Du, F., and Li, Z. (2014). Functional highly branched polymers from multicomponent polymerization (MCP) based on the ABC type Passerini reaction. *Polym. Chem.* *5*, 3316–3320.
59. Yang, B., Zhao, Y., Fu, C., Zhu, C., Zhang, Y., Wang, S., Wei, Y., and Tao, L. (2014). Introducing the Ugi reaction into polymer chemistry as a green click reaction to prepare middle-functional block copolymers. *Polym. Chem.* *5*, 2704–2708.
60. Lee, I.H., Kim, H., and Choi, T.L. (2013). Cu-catalyzed multicomponent polymerization to synthesize a library of Poly(N-sulfonylamidines). *J. Am. Chem. Soc.* *135*, 3760–3763.
61. Lee, M.H., Yang, Z., Lim, C.W., Lee, Y.H., Dongbang, S., Kang, C., and Kim, J.S. (2013). Disulfide-cleavage-triggered chemosensors and their biological applications. *Chem. Rev.* *113*, 5071–5109.
62. Hoshyar, N., Gray, S., Han, H., and Bao, G. (2016). The effect of nanoparticle size on *in vivo* pharmacokinetics and cellular interaction. *Nanomedicine* *11*, 673–692.
63. Badi, N., and Lutz, J.F. (2009). PEG-based Thermogels: applicability in physiological media. *J. Control. Release* *140*, 224–229.
64. Aathimanikandan, S.V., Savariar, E.N., and Thayumanavan, S. (2005). Temperature-sensitive dendritic micelles. *J. Am. Chem. Soc.* *127*, 14922–14929.
65. Xiao, K., Li, Y., Luo, J., Lee, J.S., Xiao, W., Gonik, A.M., Agarwal, R.G., and Lam, K.S. (2011). The effect of surface charge on *in vivo* biodistribution of PEG-oligocholeic acid based micellar nanoparticles. *Biomaterials* *32*, 3435–3446.
66. Sakhiani, N.M., and Padh, H. (2013). Organelle targeting: third level of drug targeting. *Drug Des. Dev. Ther.* *7*, 585–599.
67. Jiwpanich, S., Ryu, J.H., Bickerton, S., and Thayumanavan, S. (2010). Noncovalent encapsulation stabilities in supramolecular nanoassemblies. *J. Am. Chem. Soc.* *132*, 10683–10685.
68. Liu, B., and Thayumanavan, S. (2017). Importance of evaluating dynamic encapsulation stability of amphiphilic assemblies in serum. *Biomacromolecules* *18*, 4163–4170.